Stringent Control Over Cytoplasmic and Membrane Densities Defines Cell Geometry in *Escherichia coli*

Griffin Chure[1], Roshali T. de Silva[1], Richa Sharma[1], Michael C. Lanz[1,2], and Jonas Cremer[1,3]

[1]Department of Biology, Stanford University, Stanford, CA, USA
[2]Chan-Zuckerberg Biohub, San Francisco, CA, USA
[3]jonas.cremer@stanford.edu

October 29, 2023

Abstract

Understanding how cells regulate their growth rate, macromolecular composition, and size have been central topics in the study of microbial physiology for the better part of a century. However, we lack a mechanistic understanding of how cells so tightly coordinate biosynthesis and size control across diverse environments. In this work, we present a biophysical model of cell size control that quantitatively predicts how rod-shaped bacterial cells such as *E. coli* regulate their surface-to-volume ratio as a function of their composition. Central to this theory is a biochemical constraint that the protein density within the cell membranes and the macromolecular density within the cell cytoplasm are strictly controlled and kept at a constant ratiometric value. Through a reanalysis of more than 30 published data sets coupled with our own experiments, we demonstrate that this theory quantitatively predicts how the surface-to-volume ratio scales with the total RNA-to-protein ratio. We further test and confirm this theory by directly adjusting the RNA-to-protein ratio through genetic control of cellular ppGpp concentrations. This work demonstrates that cellular composition, rather than the growth rate, drives the regulation of cell geometry and provides a candidate biophysical mechanism for how cell size homeostasis is manifest.

1 Introduction

Microbial cells are remarkably plastic biochemical assemblies, demonstrating large-scale changes in composition and mass across diverse environments, yielding a broad range of growth rates.[1–3] Furthermore, microbes control their size and shape in concert with their growth rate,[4–7] suggesting that a strong link can be made between size and the wholesale composition of the cell. Despite this, these phenomena have been studied largely in isolation for decades, culminating in a set of phenomenological “growth laws" which quantitatively examine how cellular composition and geometry independently relate to the steady-state growth rate.

One such growth law, extensively characterized in *E. coli*, is the observation that the RNA-to-protein ratio is strongly correlated with the growth rate across diverse conditions [Fig. 1(A)]. Through experimental[8–12] and theoretical[13–19] dissection, this dependence has been rationalized as consequence of the precise

coregulation of metabolism and protein synthesis that allows cells to rapidly proliferate across environments. In a similar vein, the apparent exponential relationship between the population-averaged cell volume and growth rate [Fig. 1(B)] has been the subject of intense theoretical and experimental scrutiny,[5,6,20–29] though a consensus view has not yet emerged. While the molecular details remain enigmatic, the prevailing hypothesis[20,30] is that control and homeostasis of cell size across the cell cycle results from the precise coordination between the initiation of DNA replication, growth, and the time between initiation of replication and cell division. The regulation of protein synthesis plays a minor if not negligible role.

In this work, we present an alternative model of cell size control across environments centered on the regulation of protein synthesis and independent of DNA replication. Rather, we argue that cell size control emerges as a consequence of maintaining constant macromolecular densities across growth conditions. Driven by the empirical observation that both the total drymass density and membrane protein areal density are invariant across growth conditions, we derive a simple model which predicts that the cellular surface-to-volume ratio S_A/V is inversely proportional to the RNA-to-protein ratio thereby linking the compositional and dimensional growth laws. Through a survey of literature data and our own measurements of cell size and composition in *E. coli*, we find this theory is quantitatively predictive and accurately captures the observed scaling of S_A/V across an order of magnitude variation in growth rate. With the maintenance of macromolecular densities as a central biophysical principle, we propose a view of cell size control that concretely links the growth laws under a single theoretical framework.

2 Results

2.1 Density Maintenance as a Physiological Principle

Living matter is constrained by fundamental chemical and physical limits. For example, while cells coordinate and regulate myriad chemical reactions to facilitate growth and proliferation, the individual rates of these reactions are highly sensitive to the physicochemical details of their surroundings, including the density of macromolecules within cellular compartments.[31–33] As a result, it has been suggested that cells have evolved to operate in a narrow “optimal" density regime.[34–36] This hypothesis is well supported by a litany of observations that the total cellular drymass density[1,37–44] [and, by extension, the cytoplasmic drymass (Appendix 1)] is exceptionally tightly maintained across a variety of growth conditions [Fig. 1(C)].

Beyond biochemical reaction rates, macromolecular densities have further been shown to impact cellular ultrastructure, including the chromatin[45–47] and membranes.[48–51] As there are enumerable interfacial interactions between the cytoplasmic and membrane components (such as transport reactions and chemosensory signaling), it is plausible that densities of proteins within the cell membrane may be similarly constrained across growth conditions.[52,53] Based on a collection of proteomics data sets[54–60] and measurements on cell size[27,61–65] as well as total cellular protein,[1,41,54,56,66,67] we directly calculated the membrane protein density using a Bayesian inferential model to quantify the corresponding uncertainty [Fig. S2 and Appendix 2]. In line with our hypothesis, we find that the membrane protein density is very well constrained across growth conditions [Fig. 1(D)]. Furthermore, we find that this constancy is not simply a result of averaging as both the inner and outer membrane densities independently are tightly constrained [Fig. S3].

Further quantification shows that both densities are remarkably tightly constrained with median values

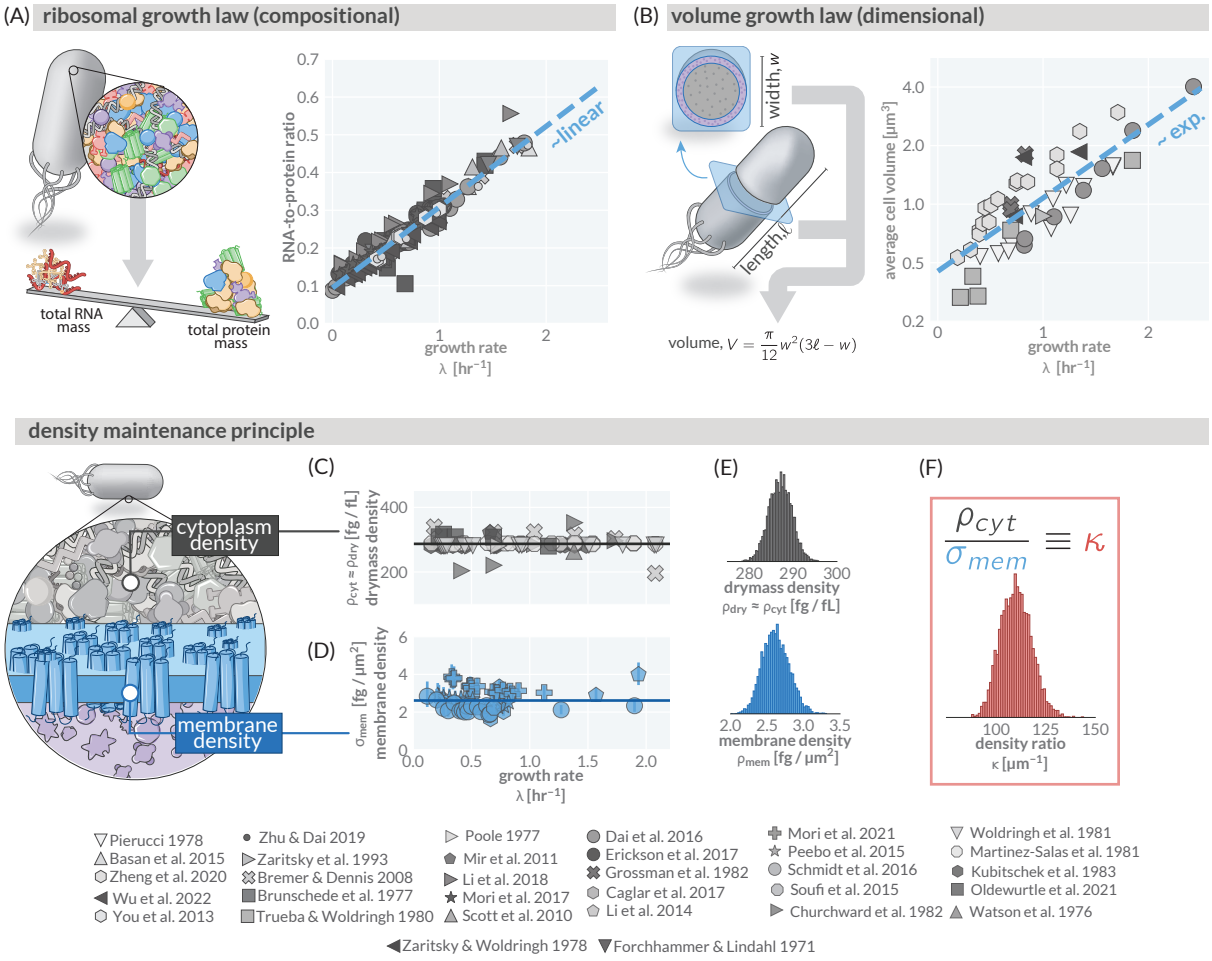

Figure 1: Cellular "growth laws" of *E. coli* and the principle of density maintenance. (A) The ribosomal growth law relates the composition of the proteome and RNA between ribosomes and non-ribosomal proteins as a function of the steady state growth rate λ, modulated here primarily through growth on different carbon sources. (B) The volume growth law relates the scaling of cellular dimensions as a function of the growth rate. The corresponding scaling behavior of width w and length ℓ is shown in Fig. S1. The drymass density (C) and the protein density within the cell membrane(s) (D) are held remarkably constant as a function of the growth rate. (E) Empirical posterior probability distributions of the cytoplasmic macromolecular density (top) and total membrane protein density (bottom) inferred from data in (C) and (D), respectively. (F) The ratio of these posterior distributions yields a density ratio κ with a median value of ≈ 106 μm^{-1}.

of $\rho_{cyt} = 287.09^{+5.26}_{-5.21}$ fg / fL and $\sigma_{mem} = 2.7^{+0.4}_{-0.3}$ fg / μm^2 [Fig. 1(E)] where the sub- and super-scripts denote the lower and upper bounds of the 95% credible regions. As both of these quantities are constant across growth rates, their ratio κ is also constant with an approximate value $\rho_{cyt}/\sigma_{mem} \equiv \kappa = 106^{+15}_{-14}$ μm^{-1} [Fig. 1(F)], and represents a measure of density maintenance between cellular compartments.

2.2 Deriving a Theory of Density Maintenance

To understand the physiological meaning of density maintenance, we mathematically examined how cytoplasmic and membrane densities relate to cell geometry. By definition, the membrane protein density σ_{mem}

depends on the total mass of membrane proteins $M_{prot}^{(mem)}$ and the total membrane area,

$$\sigma_{mem} = \frac{M_{prot}^{(mem)}}{2S_A}, \tag{1}$$

where S_A represents the cell surface area and the prefactor of 2 reflects the fact that *E. coli* has two narrowly spaced membrane layers.[68] Similarly, the cytoplasmic drymass density ρ_{cyt} follows from the masses of the cytoplasmic molecules and the cell volume V,

$$\rho_{cyt} = \frac{M_{RNA} + M_{DNA} + M_{prot}^{(cyt)} + \ldots}{V}, \tag{2}$$

where M_{RNA} and M_{DNA} represent the masses of total RNA and DNA, respectively, and the ellipses (…) denote all other molecules (lipids, metabolites, etc). Making the well-supported approximation that total RNA, DNA, and protein constitute the vast majority of total drymass,[1] the density ratio κ can be defined as

$$\kappa \equiv \frac{\rho_{cyt}}{\sigma_{mem}} = \frac{M_{RNA} + M_{DNA} + M_{prot}^{(cyt)}}{M_{prot}^{(mem)}} \times \frac{2S_A}{V}. \tag{3}$$

Thus the density ratio κ can be thought of as a composition-dependent modification of the surface-to-volume ratio S_A/V, a quantity that has been proposed as a state variable that cells directly monitor and control.[5]

It is often easier experimentally to measure the relative mass of a protein X to the mass of the proteome as a whole, $\phi_x = M_X/M_{prot}^{(tot)}$, rather than its *absolute* mass M_X. Taking that the total proteome is composed of cytoplasmic, periplasmic, and membrane proteins, it then follows that

$$M_{prot}^{(cyt)} = M_{prot}^{(tot)}(1 - \phi_{mem} - \phi_{peri}), \tag{4}$$

where ϕ_{mem} and ϕ_{peri} represent the proteome fractions of membrane and periplasmic proteins, respectively.

Making this substitution and solving Eq. 3 for the surface-to-volume ratio S_A/V (see Methods) then yields

$$\frac{S_A}{V} = \frac{\phi_{mem}\kappa}{2\left[1 + \frac{M_{RNA}}{M_{prot}^{(tot)}} - \phi_{mem} - \phi_{peri}\right]}, \tag{5}$$

where we make the approximation that the total mass of DNA is small compared to the total protein mass[1]($\frac{M_{DNA}}{M_{prot}^{(tot)}} \lesssim 0.05$). This equation, schematized in Fig. 2(A), presents a simple argument for how the surface-to-volume ratio S_A/V should scale with respect to the RNA-to-protein ratio $\frac{M_{RNA}}{M_{prot}^{(tot)}}$ and proteome composition, thereby linking cellular composition with cell geometry. Beyond being independent of the cell growth rate, we stress that this theory requires knowledge of *only* the protein and RNA composition, and *not* the DNA content, thereby being ignorant of DNA replication as a process.

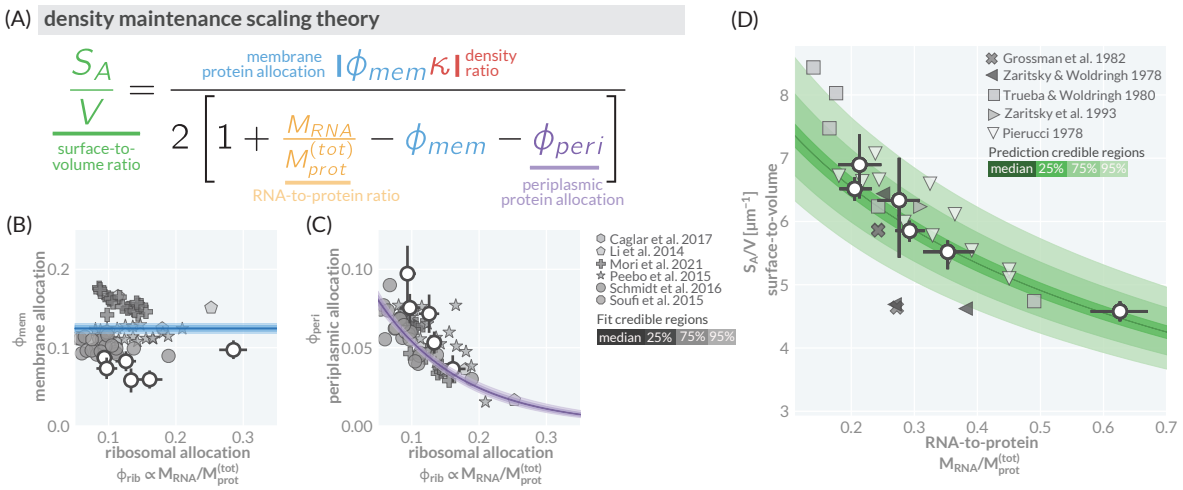

Figure 2: A density maintenance theory quantitatively predicts changes in cell dimensions as a function of cellular composition and proteome allocation. (A) The density maintenance theory as derived in the main text with RNA-to-protein ratio, and membrane/periplasmic proteome fractions (ϕ_{mem} and ϕ_{peri}) highlighted in gold, blue, and purple, respectively. The dependence of (B) ϕ_{mem} and (C) ϕ_{peri} on the ribosomal proteome fraction ϕ_{rib}, which is proportional to the RNA-to-protein ratio $\frac{M_{RNA}}{M_{prot}^{(tot)}}$, as obtained from the analysis of different proteomics data (gray markers) and own measurements (white-faced circles). Shaded lines show the inferred dependence, assuming a constant allocation of ϕ_{mem} and a variable ϕ_{peri}. (D) Predicted scaling (shaded green bands) of the cellular surface-to-volume ratio overlaid with inferred literature data (shaded markers) and our own data (white-faced circles). Error bars on measurements from this study represent the extent of the 95% credible regions of the parameter estimate while the circles represent the median value of the posterior distribution. Shaded bands in (D) represent the bounds of the 95%, 75%, 25%, and median percentiles of the posterior prediction.

2.3 Measurements of Surface-To-Volume Agrees With Density Maintenance Theory

Following our theory, the surface-to-volume ratio S_A/V is dependent on three key parameters–the proteome fractions ϕ_{mem} and ϕ_{peri}, and the RNA-to-protein ratio $\frac{M_{RNA}}{M_{prot}^{(tot)}}$. As the RNA-to-protein ratio is directly proportional to the ribosomal proteome fraction ϕ_{rib},[9,17] we can examine how membrane and periplasmic proteins are co-regulated with ribosomal components. Again leveraging recently published proteomics data, we find that the membrane and periplasmic proteome fractions have different scaling relationships with the ribosomal content [Fig. 2(B-C, shaded markers)]. We note that while there is variation between studies, the observed scaling within each data set is notably conserved. First, we observe that the membrane proteome fraction is a fixed quantity at $\phi_{mem} = 0.131^{+0.006}_{-0.006}$ (blue lines), suggesting that while the expression of individual membrane components may vary across conditions,[69] the total membrane protein fraction is fixed. Secondly, we observe that the periplasmic protein allocation is negatively correlated with the ribosomal proteome fraction, ranging between ≈ 0.1 and ≈ 0.01 across a three fold variation in ribosomal content [Fig. 2(C)]. Further interrogating this dependence we found that it is well described by a constant mass of periplasmic protein per cell ($m_{peri} = 10^{+1}_{-1}$ fg) that is independent of growth condition [Fig. S4 and Appendix 3.3]. This assumption yields accurate representation of the dependence of ϕ_{peri} on the ribosomal proteome fraction ϕ_{rib} [Fig. 2(C, purple lines)].

With estimates for κ, ϕ_{mem}, and ϕ_{peri} and their scaling with $\frac{M_{RNA}}{M_{prot}^{(tot)}}$ in hand, we have the parametric knowledge necessary to draw predictions of how S_A/V scales as a function of the RNA-to-protein ratio, illustrated by the shaded green bands in Fig. 2(D). Using the empirical ribosomal growth law [Fig. 1(A)], we estimated the RNA-to-protein ratio for a slew of surface-to-volume measurements from the literature[61–65] [Appendix

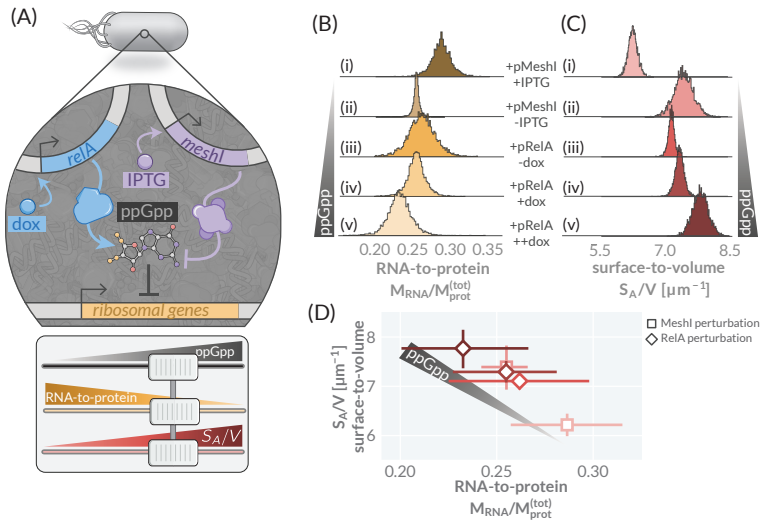

Figure 3: Perturbing ppGpp levels predictably alters the surface-to-volume ratio. (A, top) The genetic system as adapted from Büke *et al.*[70] allowing for inducible control over intracellular ppGpp concentrations. (A, bottom) The predicted effect on RNA-to-protein and surface-to-volume ratios upon changes in intracellular ppGpp concentrations. The inferred posterior probability distributions for each construct and induction condition for (B) the RNA-to-protein and (C) the surface-to-volume ratios. (D) Anticorrelation of median values of distributions shown in (B) and (C). Error bars in (D) represent the extent of the 95% credible region of the parameter estimates.

1] and found notable agreement with the prediction [Fig. 2(D, shaded points)].

Thus far, all characterization of the model has been performed using a combination of different measurements from the literature. To further test the predictive power of the theory, we independently measured the RNA-to-protein ratio $\frac{M_{RNA}}{M_{prot}^{(tot)}}$ and cell size parameters for growth on six different carbon sources. To directly measure the protein fractions ϕ_{mem} and ϕ_{peri} for these conditions, we further developed and applied biochemical assays that utilize osmotic shocks, ultracentrifugation, and protein quantification methods to separate and quantify protein fractions. Detailed protocols and controls are discussed in Appendix 3, with a brief description provided in the Methods. As our experimental data is not used in the inference of *any* of the model parameters, these measurements serve as a direct test of the theory and we find they stand in excellent agreement with the theoretical predictions [Fig. 2, white-faced circles]. Together, our measurements and the reanalysis of literature data strongly support a hypothesis that density maintenance defines the cellular surface-to-volume.

2.4 Perturbations of Intracellular ppGpp Concentrations Predictably Alter Cellular Geometry

The density maintenance theory predicts that modulation of the RNA-to-protein ratio shifts the surface-to-volume ratio in a manner that is independent of the particular growth condition. The RNA-to-protein ratio is predominantly regulated via guanosine tetraphosphate (ppGpp) which regulates the expression of a large battery of genes, including those encoding for ribosomal proteins and rRNA,[71–74] and has recently been shown to play a role in cell size control.[70] Thus, we hypothesize that controlling intracellular ppGpp concentrations should influence the surface-to-volume by altering the RNA-to-protein ratio, as predicted by the density maintenance theory. We sought to test this hypothesis using a genetic construct developed by Büke *et al.* which modulates ppGpp concentrations via induction of RelA and MeshI, enzymes involved in the synthesis and degradation of ppGpp, respectively [Fig. 3(A)]. In a single growth condition (a glucose-supplemented minimal medium), we titrated the expression of these enzymes and measured the RNA-to-protein and the surface-to-volume ratios.

Using our ensemble of measurements, we employed a Bayesian inferential model to infer the posterior probability distributions for the RNA-to-protein [Fig. 3(B)] and the surface-to-volume [Fig. 3(C)] ratios. We found that decreasing ppGpp via induction of MeshI [Fig. 3(C,i)] or increasing ppGpp via induction of RelA

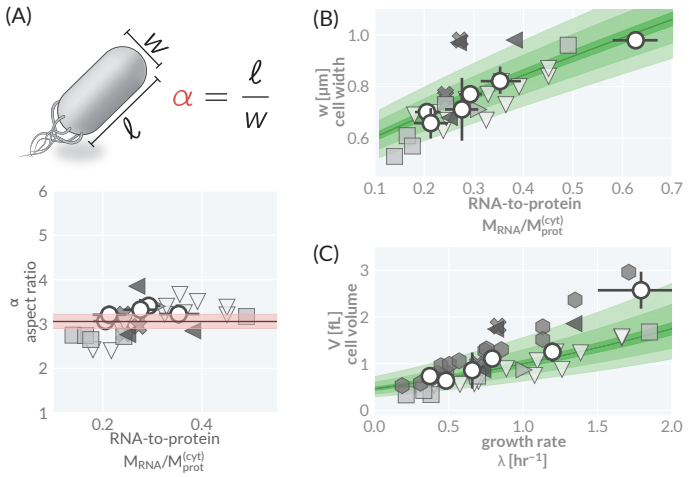

Figure 4: Aspect-ratio maintenance permits prediction of the volume growth law. (A) The average cellular aspect ratio between width and length is largely independent of the cellular composition. Light and dark red bands represent the 95% credible region and median estimate of the posterior probability distribution. (B) Predicted scaling of cell width with the RNA-to-protein ratio assuming a constant average aspect ratio. (C) The predicted and observed volume as a function of the growth rate, assuming the ribosomal growth law [Fig. 1(A), dashed line]. White-faced points represent median values of the inferred posterior distributions from our measurements for growth on different carbon sources, with error bars representing the bounds of the 95% credible region. Shaded symbols are the same as those listed in the legends of Fig. 1 and Fig. 2. Shaded green bands in (B and C) represent the bounds of the 95%, 75%, 25%, and median credible regions of the prediction.

[Fig. 3 (C, iv-v)] resulted in an increase or decrease in the RNA-to-protein ratio compared to the uninduced conditions [Fig. 3(C, ii-iii)], respectively. We further observed a increase in the surface-to-volume ratio with an increase in ppGpp concentration [Fig. 3(C)]. Plotting the surface-to-volume versus the RNA-to-protein ratios of each induction condition against each other [Fig. 3](D) reveals a strong anticorrelation between them, in line with our hypothesis under the density maintenance theory. In summary, these findings strongly supports the claim that cell geometry is set by the cell composition, and not the details of the particular growth condition.

2.5 Control of Aspect Ratio Permits a Union of the Ribosomal and Volume Growth Laws

The density maintenance theory concretely captures how the surface-to-volume ratio scales with the average cellular composition. However, cells also show exquisite control over their absolute cell dimensions–as demonstrated by the volume growth law [Fig. 1(B)]–suggesting another layer of regulation must take place. However, while the cell size varies considerably across conditions [Fig. S1], *E. coli* takes on a very characteristic rod shape with an average length approximately three times its average width.[75,76] We note that this property, the length-to-width aspect ratio α, is narrowly constrained across many growth conditions and independent of the RNA-to-protein ratio [Fig. 4(A)].

If the aspect ratio, like the density ratio κ, is held constant across conditions, the density maintenance theory can be easily extended to make predictions of absolute cell dimensions. First, we note that the surface-to-volume ratio is inversely proportional to the average width (derived in Methods),

$$\frac{S_A}{V} = \frac{12\alpha}{3\alpha - 1} \times \frac{1}{w}. \tag{6}$$

Using this, we can extend the density maintenance theory to predict average cell width from the cellular composition,

$$w = \frac{24\alpha}{3\alpha - 1} \times \frac{1 + \frac{M_{RNA}}{M_{prot}^{(tot)}} - \phi_{mem} - \phi_{peri}}{\phi_{mem}\kappa}. \tag{7}$$

Like the surface-to-volume ratio, we find excellent agreement between the predicted cell width and a combination of our own measurements and literature data [Fig. 4(B)].

With a constant average aspect ratio, the density maintenance theory can be used to describe the relationship between cell volume and the RNA-to-protein ratio. As the relationship between the RNA-to-protein ratio and the bulk growth rate is well understood,[14,16,17] this allows us to predict how cell volume scales as a function of the growth rate [Fig. 4(C)], therefore rationalizing the volume growth law [Fig. 1(B)] without invoking DNA replication.

3 Discussion

In this work, we take a holistic approach towards understanding the coregulation between cellular composition and size. We provide a concrete, biophysical principle at the center of this regulation–that macromolecular densities within the cytoplasm and the areal density of proteins in the cell membrane are held within a narrow range. Following a simple mathematical derivation based on the definition of these densities, we find that this principle imposes strong constraints on the cellular geometry, namely the surface-to-volume ratio. Through a thorough reanalysis of literature spanning nearly half a century, coupled with our own biochemical measurements, we demonstrate that this theory of density maintenance quantitatively predicts how the surface-to-volume ratio is dependent on the RNA-to-protein ratio with remarkable precision. Importantly, this approach demonstrates that cell composition, and *not* bulk growth-rate, is a major determining factor of cell size control.

Beyond our own analysis, we find that a theory of density maintenance stands in good agreement with other literature examining what does (and does not) alter cell size across conditions. For example, Basan *et al.*[21] used a series of perturbations, including the extreme overexpression of a non-needed cytoplasmic protein, to drastically change composition. As anticipated by our theory, Basan *et al.* observed that the average cell size increased considerably while total drymass density was maintained. Furthermore, as our theory does not include any rate parameters or binding constants, we would expect its predictions to be independent of temperature. Indeed, this is consistent with previous studies showing that cell composition and size are both well-maintained across temperatures, while the growth rate is strongly temperature dependent.[4,77–81] Finally, while we focus in this work on *E. coli*, there is evidence that density maintenance may be a more general property across the microbial world. For example, recent work in *Corynebacterium glutamicum*,[82] a gram-positive bacterium, reveals a strong correlation between the surface-to-volume ratio and the RNA-to-protein ratio that is consistent with our theoretical predictions. Similarly, the methanogenic archaeon *Methanococcus maripaludis* demonstrates a fixed composition across growth conditions and, in line with our theory, a fixed cell size.[83] In total, a hypothesis that cells prioritize the maintenance of macromolecular densities and do so through control of cell geometry is strongly supported by a litany of observations which have at times seemed incongruous.

Recently, Büke *et al.*[70] demonstrated that ppGpp directly altered average cell volume in a manner that was uncoupled from the bulk growth rate. While this study unequivocally proves a relationship between ppGpp concentration and cell size, the precise mechanism remains speculative. Our theory of density maintenance rationalizes this relationship–intracelluar ppGpp pools modulate the RNA-to-protein ratio through the regulation of expression of ribosomal rRNA and protein genes, therefore altering the composition and thus the cell geometry. Other work by Harris & Theriot[5] has proposed that the surface-to-volume ratio is a quantity that cells actively monitor and homeostatically control through the coordination of volume and

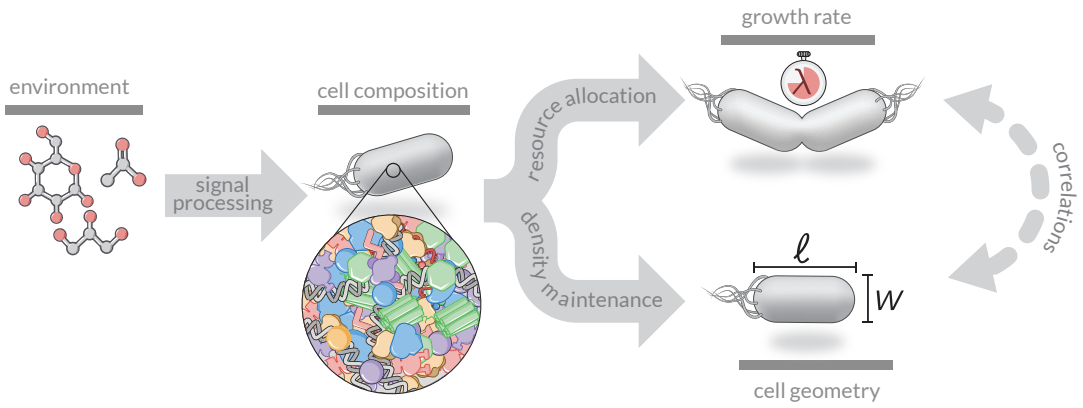

Figure 5: A revised model of cell size and growth rate regulation. Chemical details of the environment set the cellular composition through sensory pathways and integrated regulation of gene expression. Given the cellular composition, the bulk growth rate is determined via the regulation of metabolic and translational fluxes, setting cellular composition. Simultaneously and following our density maintenance theory pressure to simultanously preserve macromolecular densities within the cytoplasm and membrane protein densities within the membrane determines cellular geometry.

surface expansion. Our work provides a biophysical principle by which relative differences between these processes can be sensed. Particularly, we believe that actively monitoring the density ratio κ could provide the feedback control necessary to ensure that the surface-to-volume ratio is properly constrained. This begs two fundamental molecular questions: how could cells sense densities and how is sensing coupled to width control?

We speculate that the Rod complex lies at the heart of both of these questions. The Rod complex is a large protein assembly[84–86] found across the bacterial tree of life,[87] which rotates about the long axis of the cell along the inner membrane expanding the cell wall and, therefore, increasing the cell volume and surface area.[88,89] While lengthening the cell over the course of the cell cycle, the Rod complex also determines the width of the cell,[85,90,91] thereby controlling the surface-to-volume ratio. Thus, for densities in the cytoplasm and membrane to be effectively maintained, the activity of the Rod complexes must be directly controlled. As the Rod complex rotates through both the cytoplasmic and membrane environments, it is subjected to density-dependent forces. We thus think it is plausible that the action of the Rod complex is modulated by membrane and cytoplasmic densities to ensure coordination of length increase and width control. As genetic perturbations of various Rod complex components have been shown to strongly affect cell size and shape homeostasis,[91,92] we speculate that they may together act also as “sensor" of the relative density between the membrane and cytoplasm.

Despite evidence that growth rate regulation and cell size control are uncoupled in various situations– such as through temperature variation– growth rate is commonly viewed as a control variable for bacterial physiology as a whole. However, we argue that growth should be thought of as an emergent property of the cellular physiology, as is cell size [Fig. 5]. We view the cell composition as being set by the coordination of gene expression following from sensing of the cells’ environment and its metabolic state. Growth rate emerges from the relative rates of metabolism and translation resulting from this composition.[17] Separately, as we have demonstrated in this work, the pressure to maintain macromolecular densities within the cytoplasm and membrane compartments strongly constrains the cellular geometry. As a consequence, strong correlations between cell size and growth rate can emerge even without a direct causal link between them. Thus, approaches to understand cell physiology should not rely on growth rate as an explanatory process,

but rather the fundamental physical and chemical limits that cells must obey and can plausibly biochemically measure.

4 Methods

4.1 Full Derivation of Surface-To-Volume Density Maintenance Theory

Here we provide a step-by-step demonstration of how we arrived at Eq. 5 from the defintion of the density ratio κ. Noting that the cytoplasmic protein mass can be expressed in terms of the proteome mass fractions (Eq. 4; $M_{prot}^{(cyt)} = M_{prot}^{(tot)}(1 - \phi_{mem} - \phi_{peri})$, Eq. 3 can be expressed as

$$\kappa \equiv \frac{\rho_{cyt}}{\sigma_{mem}} = \frac{M_{RNA} + M_{DNA} + M_{prot}^{(tot)}(1 - \phi_{mem} - \phi_{peri})}{M_{prot}^{(mem)}} \times 2S_A V. \tag{8}$$

Multiplying the numerator and denominator by $1/M_{prot}^{(tot)}$ yields

$$\kappa \equiv \frac{\rho_{cyt}}{\sigma_{mem}} = \frac{\frac{M_{RNA}}{M_{prot}^{(tot)}} + \frac{M_{DNA}}{M_{prot}^{(tot)}} + \frac{M_{prot}^{(tot)}}{M_{prot}^{(tot)}}(1 - \phi_{mem} - \phi_{peri})}{\frac{M_{prot}^{(mem)}}{M_{prot}^{(tot)}}} \times \frac{2S_A}{V}. \tag{9}$$

We now note that the i) ratio $M_{prot}^{(mem)}/M_{prot}^{(tot)}$ is defined as the membrane proteome fraction ϕ_{mem} and ii) that the mass ratio of DNA to protein $M_{DNA}/M_{prot}^{(tot)}$ is small[1] and can be neglected. Doing so yields

$$\kappa \equiv \frac{\rho_{cyt}}{\sigma_{mem}} = \frac{\frac{M_{RNA}}{M_{prot}^{(tot)}} + \cancel{\frac{M_{DNA}}{M_{prot}^{(tot)}}}^{\approx 0} + \cancel{\frac{M_{prot}^{(tot)}}{M_{prot}^{(tot)}}}^{1}(1 - \phi_{mem} - \phi_{peri})}{\cancel{\frac{M_{prot}^{(mem)}}{M_{prot}^{(tot)}}}^{\phi_{mem}}} \times \frac{2S_A}{V} = \frac{\frac{M_{RNA}}{M_{prot}^{(tot)}} + 1 - \phi_{mem} - \phi_{peri}}{\phi_{mem}} \times \frac{2S_A}{V}, \tag{10}$$

which can then be solved for S_A/V to yield Eq. 5.

4.2 Mathematical Relation Between Width and the Surface-To-Volume Ratio

In Eq. 6, we assert that the surface-to-volume ratio S_A/V is inversely proportional to the cell width w. This is arrived at as follows. We state that the surface area of a spherocylinder with a width w and total length ℓ is defined as

$$S_A = \overbrace{\pi w(\ell - w)}^{\text{cylinder area}} + \underbrace{\pi w^2}_{\text{cap area}} = \pi w \ell. \tag{11}$$

Similarly, we state that the volume of a sphereocylinder is

$$V = \overbrace{\frac{\pi}{4}w^2(\ell - w)}^{\text{cylinder volume}} + \underbrace{\frac{\pi}{6}w^3}_{\text{cap volume}} = \frac{\pi}{12}w^3(3\ell - w). \tag{12}$$

As a result, the surface-to-volume of a sphereocylinder is

$$\frac{S_A}{V} = \frac{\pi\ell w}{\frac{\pi}{12}w^2(3\ell - w)} = \frac{12\ell}{w(3\ell - w)}. \tag{13}$$

We can now state that a spherocylinder has a length-to-width aspect ratio α, simplifying Eq. 13 as

$$\frac{S_A}{V} = \frac{12\alpha w}{w^2(3\alpha - 1)} = \frac{12\alpha}{3\alpha - 1} \times \frac{1}{w}, \tag{14}$$

which is the same as Eq. 6. As the aspect ratio α is typically 2 or larger, the surface-area-to-volumre ratio is in a good approximation only dependent on width, $\frac{S_A}{V} \approx \frac{4}{w}$.

4.3 Bayesian Parameter Estimation

We employed a Bayesian definition of probability to infer the various parameters used in this study. We direct the reader to the Appendix 2for a detailed discussion of these statistical models and their assumptions. Speaking generally, we sought to compute the posterior probability distribution $g(\theta \mid y)$ of a parameter θ conditioned on a set of measurements y. Using Bayes' rule, this can be computed as

$$g(\theta \mid y) = \frac{f(y \mid \theta)g(\theta)}{f(y)}, \tag{15}$$

where g and f denote probability density functions over parameter and data, respectively. For the data observed in this work, we used a Gaussian distribution for the likelihood function $f(y \mid \theta)$ for the parameter(s) of interest. The choice of the prior distribution $g(\theta)$ was dependent on the precise parameter being inferred, but in most cases was treated to be a standard half-normal distribution with a scale parameter of $\sigma = 1$. For this work, the denominator $f(y)$ was treated as a normalization constant and was therefore neglected in the estimation. All statistical modeling and parameter inference was performed using Markov chain Monte Carlo (MCMC). Specifically, we used Hamiltonian Monte Carlo sampling as is implemented in the Stan programming language.[93] All statistical models as `stan` files are available on the paper's GitHub repository accessible via doi:10.5281/zenodo.10048570.

4.4 Bacterial Strains and Cell Husbandry

Experiments performed in this work were conducted using *Escherichia coli* K-12 strain NCM3722 supplied from the lab of Terence Hwa at UCSD, originally obtained from the laboratory of Sydney Kustu.[94] Perturbations of intracellular ppGpp concentrations were performed using a genetic system as described in Büke *et al.*[70] These plasmids (without fluorescent tags) were ordered from AddGene (pRelA' AddGeneID:175595; pMeshI AddGeneID:175594) and transformed individually into our lab stock of NCM3722 on appropriate

selection conditions. All used strains are listed in Appendix Table 2. Culturing plasmids were performed under either Ampicillin (pMeshI; 100 µg / mL) or Kanamycin (pRelA; 50 µg/mL) selection. In experiments with minimal media, one third of these concentrations were used.

To ensure sample analysis at steady-state, cells were processed through three different cultivation steps before samples were taken. To start, "seed culture" was grown in Miller LB rich medium (Fisher Scientific, Cat. No. BP1426) from a single colony on an LB agarose plate. This seed culture was grown in a 37° C water-bath shaker under constant aeration (shaking at 240 rpm) for several hours until the culture was saturated. This seed culture was then diluted at least three hundred fold into fresh LB media or a minimal phosphate buffer medium (basic buffer solution supplemented with 10 mM NH_4Cl and a carbon-source of choice, see Appendix 3.1). This culture, the "pre-culture condition", was then allowed to grow under constant aeration until an optical density $OD_{600nm} \approx 0.3 - 0.4$ (Thermo Scientific Genesys 30, 1-cm path length cuvette) was reached. This culture was the diluted ten fold into fresh medium with the same composition, pre-warmed to 37° C. This culture, the "experimental culture", was then grown in identical conditions as the pre-culture. Growth curves were obtained by regular OD_{600} measurements while the culture remained between an optical density range of $OD_{600nm} \approx 0.04 - 0.5$. Experimental samples were taken and processed as described in Appendix 3and briefly below.

For strains with ppGpp perturbations, the seed culture was grown in a glucose-supplemented minimal medium. Once the seed culture reached an optical density OD_{600nm} between $0.3 - 0.4$, the culture was diluted two-thousand fold into a fresh, prewarmed glucose minimal medium supplemented with the appropriate amount of inducer, either doxycycline (dox, Sigma, Cat. No. D5207) or Isopropyl β- d-1-thiogalactopyranoside (ITPG, Goldbio Cat. No. 12481C5) for RelA and MeshI induction, respectively.

4.5 Quantification of Total RNA and Protein Masses

To obtain the RNA-to-protein ratio $\frac{M_{RNA}}{M_{prot}^{(tot)}}$ we determined total RNA and total protein separately, starting with 1ml and 1.5ml cell culture samples respectively collected at the same time from a steady-state culture at $OD_{600nm} \approx 0.4$. Total protein was determined following the biuret method.[95] Total RNA was determined following a well-established perchloric acid method[96] optimized to account for cell loss during centrifugation. Protocols are provided in Appendix 3.2.

4.6 Quantification of Periplasmic Protein Mass

To quantify periplasmic protein mass, we further developed a previously introduced protein separation assay.[97] To proceed, a 1ml sample volume was collected at $OD_{600nm} \approx 0.4$ from a steady state culture. The sample was then exposed to a mild osmotic shock to fracture the outer membrane. Periplasmic proteins accumulating in the solution where then separated from other proteins (cytoplasmic and membrane attached proteins) via centrifugation. Finally, the Biorad protein assay was used to quantify total protein mass in the periplasmic fraction (supernatant). Mass spectrometry analysis of the periplasmic protein fraction confirmed the strong enrichment of periplasmic proteins. This analysis and the detailed experimental protocols are provided in Appendix 3.3.

4.7 Quantification of Membrane Protein Mass

To quantify the mass of membrane proteins we have developed an assay which uses ultracentrifugation to separate membrane from other proteins. To proceed, 2ml culture volume was collected from a steady-state culture at $OD_{600nm} \approx 0.4$. After sonication and the separation of unlysed cells via centrifugation, ultracentrifugations at 65k RPM (100k G) was performed to extract membrane proteins. The mass of the membrane proteins (pellet) was then determined using the BCA microassay, an assay chosen to be compatible with the separation procedure. The detailed protocol is provided in Appendix 3.4.

4.8 Microscopy & Measurement of Cell Dimensions

From a steady-state culture, 2 µL was transferred onto a 1% agarose pad supplemented with isotonic minimal medium buffer base. After drying for 2 - 3 minutes, this pad was mounted on a slide, covered with a coverslip, and imaged under 100X phase-contrast microscopy using a Zeiss AxioVert 200M microsope outfitted with an AmScope MU1003 CMOS camera. Images were transferred to a back-up server and were later processed using in-house image processing Python code, as described in Appendix 4.

4.9 Code and Data Availability

All Python code, Stan probabilistic models, and processed data sets are available on the paper's GitHub repository doi:10.5281/zenodo.10048570 accessible via `github.com/cremerlab/density_maintenance`. Raw microscopy images are available to download from the Stanford Data Repository accessible via doi: 10.25740/mk520hp68790.

5 Acknowledgements

We thank Markus Arnoldini, Rohan Balakrishnan, Nathan Belliveau, Avi Flamholz, Mathis Leblanc, Shaili Mathur, Manuel Razo-Mejia, Tom Röschinger, Gabe Salmon, Masaru Shimasawa, Jan Skotheim, and Alfred Spormann for extensive discussion and critical feedback on the manuscript. We also thank Ferhat Büke and Sander Tans for providing access to data from their recent work.[70] G.C. acknowledges support by the NSF Postdoctoral Research Fellowships in Biology Program (grant no. 2010807). J.C. acknowledges support via Bio-X Seeding Grant 10-32 and a Terman Fellowship from Stanford University, USA.

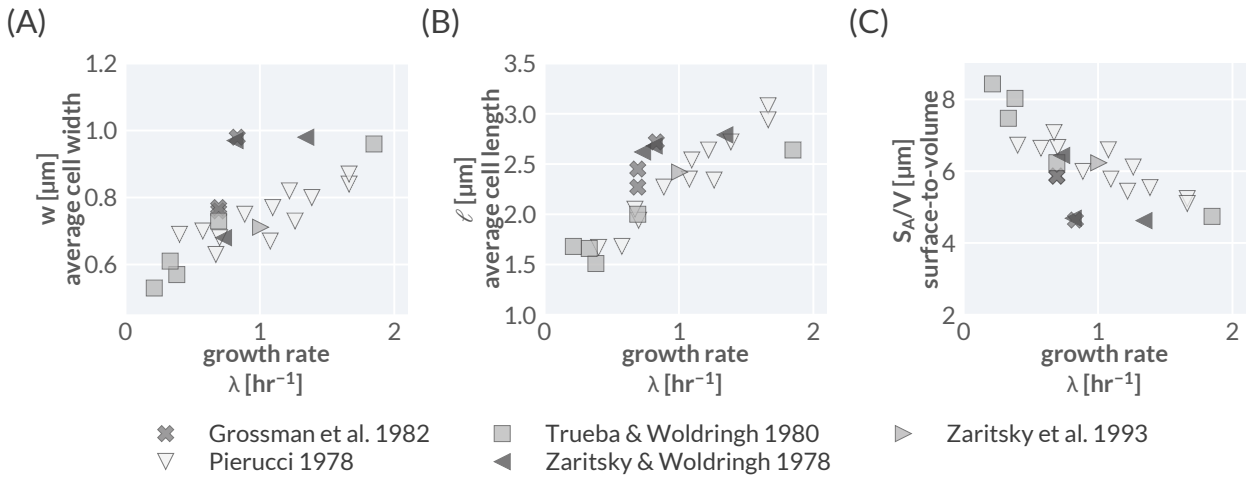

Figure S1: Other dimensional growth laws. Empirical relationships between the average cell (A) width, (B) length, and (C) surface-to-volume ratio as a function of the steady-state growth rate. Growth on different carbon sources.

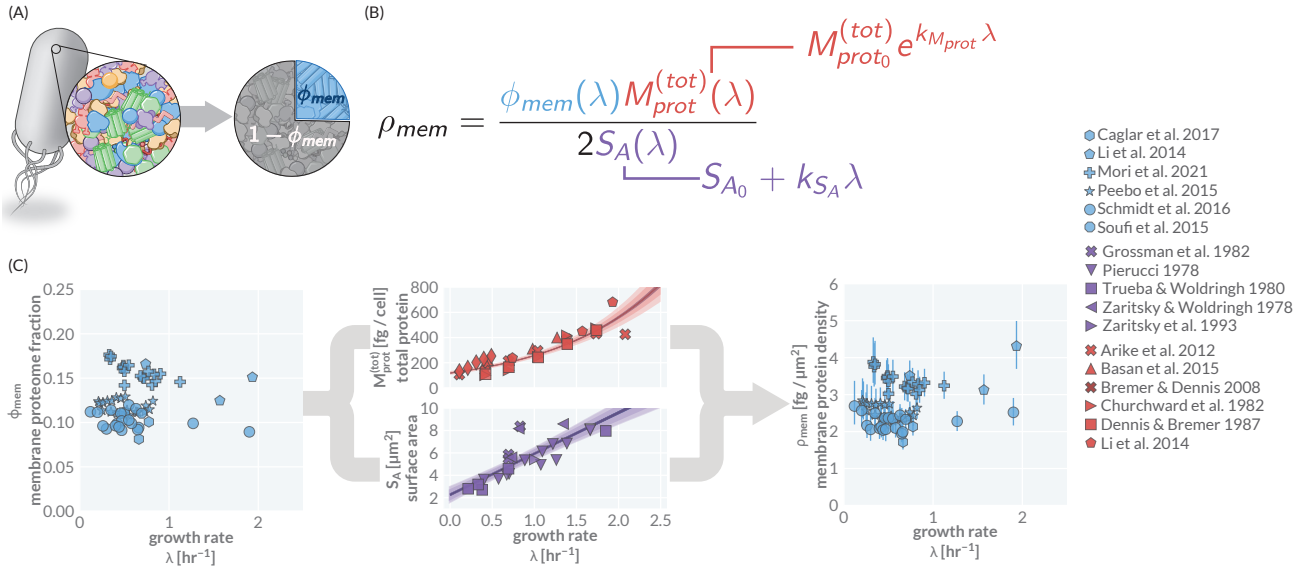

Figure S2: Calculation of membrane protein areal densities from mass spectrometry data. (A) Mass spectrometry provides data on proteome composition for the total cell, including the fraction of the proteome being membrane proteins, ϕ_{mem}. (B) For each sample in the mass spectrometry dataset, one can calculate the membrane density (black, left) knowing the total mass of protein per cell $M_{prot}^{(tot)}$ (red) and the surface area of the cell S_A (purple). The total protein mass as a function of the growth rate can be empirically well described by an exponential relation with two parameters, $M_{prot,0}^{(tot)}$ and $k_{M_{prot}}$. Similarly, the total surface area as a function of the growoth rate can be well described by a linear relation with a intercept and slope of S_{A_0} and k_{S_A}, respectively. (C) For each measurement of the membrane protein fraction (left), the total membrane protein density (right) can be calculated given uncertainty in fitting an exponential (middle, top) and linear (middle, bottom) function to the total protein and surface area, respectively, as a function of the growth rate. Shaded bands represent the 95%, 75%, 25%, and median percentiles of the fit from light to dark, respectively. Markers and errors in (C, right) denote the median and extent of the 95% credible regions calculated from the equation shown in (B).

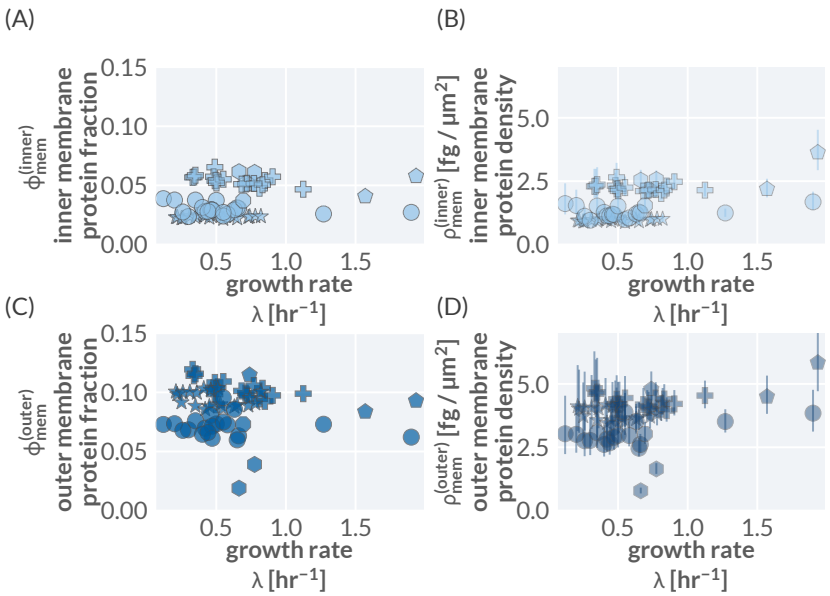

Figure S3: Membrane densities are constrained in both the inner and outer membrane. (A) Inner membrane protein fraction as observed in proteomic data using protein-level classification in Babu *et al.*[60] (B) Calculated inner membrane protein density following procedure outlined in Fig. S2. (C) Observed outer membrane protein fraction as observed in proteomic data and (D) calculated outer membrane protein density. While there is variation between studies for all quantities, the observed scaling within each data set is notably conserved. Symbols are the same as those listed in the legends of Fig. 1.

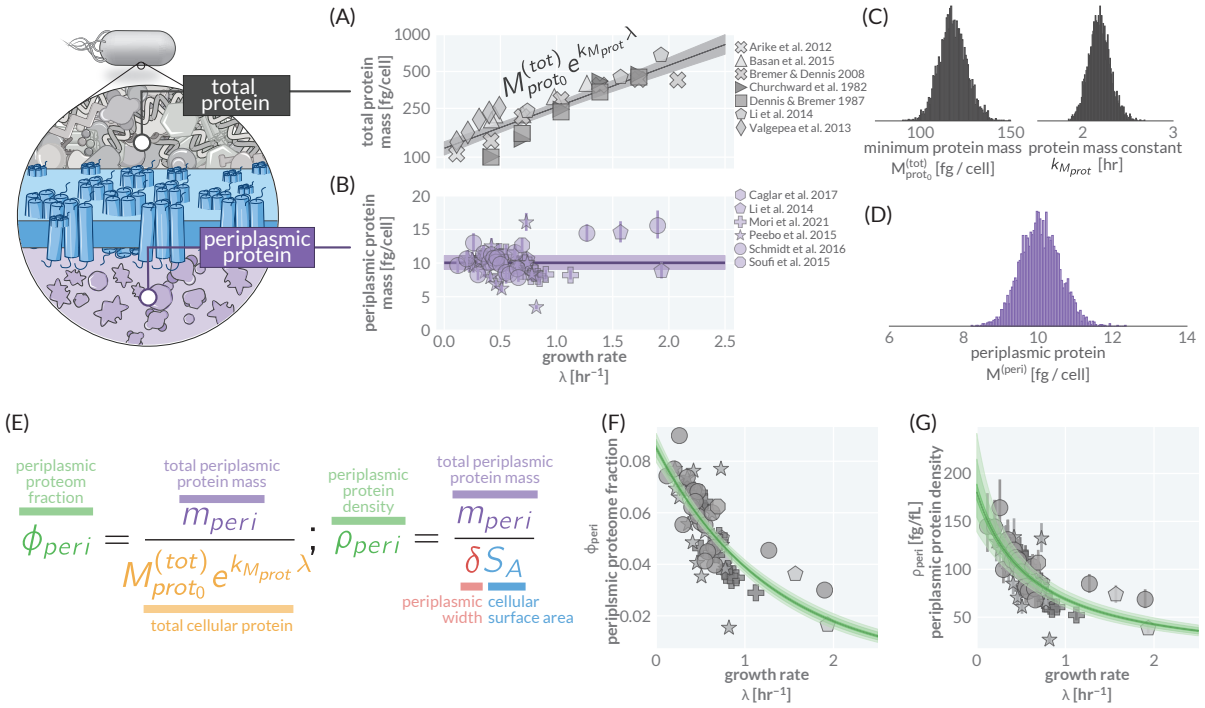

Figure S4: Characterization of the periplasmic proteome fraction and density. (A) Observed growth-rate dependence of the total cellular protein. (B) Observed total periplasmic protein mass, as calculated from proteomic data and total protein mass. Posterior probability distributions of parameters describing the exponential scaling of total protein with growth rate $M^{(tot)}{}_{prot}\, e^{k_M prot \lambda}$ (C) and for the constant periplasmic protein mass constant $M^{(per)}_{prot}$ (D). (E) Equations for predicting the total periplasmic proteome fraction and periplasmic protein density as a function of the growth rate. We assume here a constant periplasmic width $\delta = 24.6$ nm.[68] Predictions overlaid with observations for the (F) periplasmic proteome fraction and (G) the periplasmic protein density. Shaded bands in figure correspond to the 95%, 75%, 25%, and median percentiles of the posterior probability density.

References

[1] Hans Bremer and Patrick P. Dennis. Modulation of Chemical Composition and Other Parameters of the Cell at Different Exponential Growth Rates. *EcoSal Plus*, 3(1), October 2008. Publisher: American Society for Microbiology.

[2] Måns Ehrenberg, Hans Bremer, and Patrick P. Dennis. Medium-dependent control of the bacterial growth rate. *Biochimie*, 95(4):643–658, April 2013.

[3] Nathan M. Belliveau, Griffin Chure, Christina L. Hueschen, Hernan G. Garcia, Jane Kondev, Daniel S. Fisher, Julie A. Theriot, and Rob Phillips. Fundamental limits on the rate of bacterial growth and their influence on proteomic composition. *Cell Systems*, 12(9):924–944.e2, September 2021.

[4] M. Schaechter, O. Maaløe, and N. O. Kjeldgaard. Dependency on medium and temperature of cell size and chemical composition during balanced growth of *Salmonella typhimurium*. *Microbiology*, 19(3):592–606, 1958.

[5] Leigh K. Harris and Julie A. Theriot. Surface Area to Volume Ratio: A Natural Variable for Bacterial Morphogenesis. *Trends in Microbiology*, 26(10):815–832, October 2018.

[6] Sattar Taheri-Araghi, Serena Bradde, John T. Sauls, Norbert S. Hill, Petra Anne Levin, Johan Paulsson, Massimo Vergassola, and Suckjoon Jun. Cell-Size Control and Homeostasis in Bacteria. *Current Biology*, 25(3):385–391, February 2015.

[7] Suckjoon Jun, Fangwei Si, Rami Pugatch, and Matthew Scott. Fundamental principles in bacterial physiology - history, recent progress, and the future with focus on cell size control: a review. *Reports on Progress in Physics*, 81(5):056601, May 2018.

[8] Arthur L. Koch. The Adaptive Responses of Escherichia coli to a Feast and Famine Existence. In A. H. Rose and J. F. Wilkinson, editors, *Advances in Microbial Physiology*, volume 6, pages 147–217. Academic Press, January 1971.

[9] Matthew Scott, Carl W. Gunderson, Eduard M. Mateescu, Zhongge Zhang, and Terence Hwa. Interdependence of Cell Growth and Gene Expression: Origins and Consequences. *Science*, 330(6007):1099–1102, November 2010. tex.ids: scott2010a Publisher: American Association for the Advancement of Science Section: Report.

[10] Jes Forchhammer and Lasse Lindahl. Growth rate of polypeptide chains as a function of the cell growth rate in a mutant of Escherichia coli. *Journal of Molecular Biology*, 55(3):563–568, February 1971.

[11] H Brunschede, T L Dove, and H Bremer. Establishment of Exponential Growth After a Nutritional Shift-Up in *Escherichia coli* B/r: Accumulation of Deoxyribonucleic Acid, Ribonucleic Acid, and Protein. *Journal of Bacteriology*, 129:14, 1977.

[12] Nicole C. E. Imholz, Marek J. Noga, Niels J. F. van den Broek, and Gregory Bokinsky. Calibrating the Bacterial Growth Rate Speedometer: A Re-evaluation of the Relationship Between Basal ppGpp, Growth, and RNA Synthesis in Escherichia coli. *Frontiers in Microbiology*, 11, 2020.

[13] Douwe Molenaar, Rogier van Berlo, Dick de Ridder, and Bas Teusink. Shifts in growth strategies reflect tradeoffs in cellular economics. *Molecular Systems Biology*, 5(1):323, January 2009. Publisher: John Wiley & Sons, Ltd.

[14] M. Scott, S. Klumpp, E. M. Mateescu, and T. Hwa. Emergence of robust growth laws from optimal regulation of ribosome synthesis. *Molecular Systems Biology*, 10(8):747–747, August 2014.

[15] Evert Bosdriesz, Douwe Molenaar, Bas Teusink, and Frank J. Bruggeman. How fast-growing bacteria robustly tune their ribosome concentration to approximate growth-rate maximization. *The FEBS Journal*, 282(10):2029–2044, 2015. _eprint: https://febs.onlinelibrary.wiley.com/doi/pdf/10.1111/febs.13258.

[16] Nils Giordano, Francis Mairet, Jean-Luc Gouzé, Johannes Geiselmann, and Hidde de Jong. Dynamical Allocation of Cellular Resources as an Optimal Control Problem: Novel Insights into Microbial Growth Strategies. *PLOS Computational Biology*, 12(3):e1004802, March 2016. Publisher: Public Library of Science.

[17] Griffin Chure and Jonas Cremer. An optimal regulation of fluxes dictates microbial growth in and out of steady state. *eLife*, 12:e84878, March 2023. Publisher: eLife Sciences Publications, Ltd.

[18] Hugo Dourado and Martin J. Lercher. An analytical theory of balanced cellular growth. *Nature Communications*, 11(1):1226, March 2020. Number: 1 Publisher: Nature Publishing Group.

[19] Andrea Y. Weiße, Diego A. Oyarzún, Vincent Danos, and Peter S. Swain. Mechanistic links between cellular trade-offs, gene expression, and growth. *Proceedings of the National Academy of Sciences*, 112(9):E1038–E1047, March 2015. Publisher: National Academy of Sciences Section: PNAS Plus.

[20] W. D. Donachie, K. J. Begg, and M. Vicente. Cell length, cell growth and cell division. *Nature*, 264(5584):328–333, November 1976. Bandiera_abtest: a Cg_type: Nature Research Journals Number: 5584 Primary_atype: Research Publisher: Nature Publishing Group.

[21] Markus Basan, Manlu Zhu, Xiongfeng Dai, Mya Warren, Daniel Sévin, Yi-Ping Wang, and Terence Hwa. Inflating bacterial cells by increased protein synthesis. *Molecular Systems Biology*, 11(10):836, October 2015. Publisher: John Wiley & Sons, Ltd.

[22] Hai Zheng, Po-Yi Ho, Meiling Jiang, Bin Tang, Weirong Liu, Dengjin Li, Xuefeng Yu, Nancy E. Kleckner, Ariel Amir, and Chenli Liu. Interrogating the *Escherichia coli* cell cycle by cell dimension perturbations. *Proceedings of the National Academy of Sciences*, 113(52):15000–15005, December 2016. Company: National Academy of Sciences Distributor: National Academy of Sciences Institution: National Academy of Sciences Label: National Academy of Sciences Publisher: Proceedings of the National Academy of Sciences.

[23] Fangwei Si, Dongyang Li, Sarah E. Cox, John T. Sauls, Omid Azizi, Cindy Sou, Amy B. Schwartz, Michael J. Erickstad, Yonggun Jun, Xintian Li, and Suckjoon Jun. Invariance of Initiation Mass and Predictability of Cell Size in Escherichia coli. *Current Biology*, 27(9):1278–1287, May 2017.

[24] Ariel Amir. Is cell size a spandrel? *eLife*, 6:e22186, January 2017. Publisher: eLife Sciences Publications, Ltd.

[25] Manuel Campos, Sander K Govers, Irnov Irnov, Genevieve S Dobihal, François Cornet, and Christine Jacobs-Wagner. Genomewide phenotypic analysis of growth, cell morphogenesis, and cell cycle events in *Escherichia coli*. *Molecular Systems Biology*, 14(6), June 2018. tex.ids: campos2018a.

[26] Fangwei Si, Guillaume Le Treut, John T. Sauls, Stephen Vadia, Petra Anne Levin, and Suckjoon Jun. Mechanistic Origin of Cell-Size Control and Homeostasis in Bacteria. *Current Biology*, 29(11):1760–1770.e7, June 2019.

[27] Hai Zheng, Yang Bai, Meiling Jiang, Taku A. Tokuyasu, Xiongliang Huang, Fajun Zhong, Yuqian Wu, Xiongfei Fu, Nancy Kleckner, Terence Hwa, and Chenli Liu. General quantitative relations linking cell growth and the cell cycle in Escherichia coli. *Nature Microbiology*, 5(8):995–1001, August 2020. Number: 8 Publisher: Nature Publishing Group.

[28] Sander K. Govers, Manuel Campos, Bhavyaa Tyagi, Géraldine Laloux, and Christine Jacobs-Wagner. Apparent simplicity and emergent robustness in bacterial cell cycle control, January 2023. Pages: 2023.01.16.524295 Section: New Results.

[29] Sriram Tiruvadi-Krishnan, Jaana Männik, Prathitha Kar, Jie Lin, Ariel Amir, and Jaan Männik. Coupling between DNA replication, segregation, and the onset of constriction in Escherichia coli. *Cell Reports*, 38(12):110539, March 2022.

[30] Stephen Cooper and Charles E. Helmstetter. Chromosome replication and the division cycle of Escherichia coli Br. *Journal of Molecular Biology*, 31(3):519–540, February 1968.

[31] Alexander M. Berezhkovskii and Attila Szabo. Theory of Crowding Effects on Bimolecular Reaction Rates. *The Journal of Physical Chemistry B*, 120(26):5998–6002, July 2016.

[32] Jose L. Alejo, Christopher P. Kempes, and Katarzyna P. Adamala. Diffusion control in biochemical specificity. *Biophysical Journal*, 121(8):1541–1548, April 2022. Publisher: Elsevier.

[33] Bert Poolman. Physicochemical homeostasis in bacteria. *FEMS Microbiology Reviews*, 47(4):fuad033, July 2023.

[34] K. A. Dill, K. Ghosh, and J. D. Schmit. Physical limits of cells and proteomes. *Proceedings of the National Academy of Sciences*, 108(44):17876–17882, November 2011.

[35] Alexei Vazquez. Optimal macromolecular density in the cell. *Proceedings of the National Academy of Sciences*, 109(9):E533–E533, February 2012. Publisher: Proceedings of the National Academy of Sciences.

[36] Tin Yau Pang and Martin J. Lercher. Optimal density of bacterial cells. *PLOS Computational Biology*, 19(6):e1011177, June 2023. Publisher: Public Library of Science.

[37] Enno R. Oldewurtel, Yuki Kitahara, and Sven van Teeffelen. Robust surface-to-mass coupling and turgor-dependent cell width determine bacterial dry-mass density. *Proceedings of the National Academy of Sciences*, 118(32), August 2021. Publisher: National Academy of Sciences Section: Physical Sciences.

[38] H E Kubitschek, W W Baldwin, and R Graetzer. Buoyant density constancy during the cell cycle of Escherichia coli. *Journal of Bacteriology*, 155(3):1027–1032, September 1983. Publisher: American Society for Microbiology.

[39] Mustafa Mir, Zhuo Wang, Zhen Shen, Michael Bednarz, Rashid Bashir, Ido Golding, Supriya G. Prasanth, and Gabriel Popescu. Optical measurement of cycle-dependent cell growth. *Proceedings of the National Academy of Sciences*, 108(32):13124–13129, August 2011. Publisher: Proceedings of the National Academy of Sciences.

[40] S W Watson, T J Novitsky, H L Quinby, and F W Valois. Determination of bacterial number and biomass in the marine environment. *Applied and Environmental Microbiology*, 33(4):940–946, April 1977.

[41] Gordon Churchward, Hans Bremer, and Ry Young. Macromolecular composition of bacteria. *Journal of Theoretical Biology*, 94(3):651–670, February 1982.

[42] C. L. Woldringh, N. B. Grover, R. F. Rosenberger, and A. Zaritsky. Dimensional rearrangement of rod-shaped bacteria following nutritional shift-up. II. Experiments with Escherichia coliBr. *Journal of Theoretical Biology*, 86(3):441–454, October 1980.

[43] R. K. Poole. Fluctuations in Buoyant Density during the Cell Cycle of Escherichia coli K12: Signiacance for the Preparation of Synchronous Cultures by Age Selection. *Microbiology*, 98(1):177–186, 1977. Publisher: Microbiology Society,.

[44] E Martínez-Salas, J A Martín, and M Vicente. Relationship of Escherichia coli density to growth rate and cell age. *Journal of Bacteriology*, 147(1):97–100, July 1981.

[45] Juin Kim, Chanil Jeon, Hawoong Jeong, Youngkyun Jung, and Bae-Yeun Ha. A polymer in a crowded and confined space: effects of crowder size and poly-dispersity. *Soft Matter*, 11(10):1877–1888, 2015. Publisher: Royal Society of Chemistry.

[46] Renko de Vries. DNA condensation in bacteria: Interplay between macromolecular crowding and nucleoid proteins. *Biochimie*, 92(12):1715–1721, December 2010.

[47] Barak Akabayov, Sabine R. Akabayov, Seung-Joo Lee, Gerhard Wagner, and Charles C. Richardson. Impact of macromolecular crowding on DNA replication. *Nature Communications*, 4(1):1615, March 2013. Number: 1 Publisher: Nature Publishing Group.

[48] Maryna Löwe, Milara Kalacheva, Arnold J. Boersma, and Alexej Kedrov. The more the merrier: effects of macromolecular crowding on the structure and dynamics of biological membranes. *The FEBS Journal*, 287(23):5039–5067, 2020. _eprint: https://onlinelibrary.wiley.com/doi/pdf/10.1111/febs.15429.

[49] Gernot Guigas and Matthias Weiss. Effects of protein crowding on membrane systems. *Biochimica et Biophysica Acta (BBA) - Biomembranes*, 1858(10):2441–2450, October 2016.

[50] David Garenne, Albert Libchaber, and Vincent Noireaux. Membrane molecular crowding enhances MreB polymerization to shape synthetic cells from spheres to rods. *Proceedings of the National Academy of Sciences*, 117(4):1902–1909, January 2020.

[51] Jeanne C. Stachowiak, Eva M. Schmid, Christopher J. Ryan, Hyoung Sook Ann, Darryl Y. Sasaki, Michael B. Sherman, Phillip L. Geissler, Daniel A. Fletcher, and Carl C. Hayden. Membrane bending by protein–protein crowding. *Nature Cell Biology*, 14(9):944–949, September 2012. Number: 9 Publisher: Nature Publishing Group.

[52] M. Aldea, E. Herrero, M. I. Esteve, and R. Guerrero. Surface density of major outer membrane proteins in Salmonella typhimurium in different growth conditions. *Journal of General Microbiology*, 120(2):355–367, October 1980.

[53] Nathan M. Belliveau, Stephanie L. Barnes, William T. Ireland, Daniel L. Jones, Michael J. Sweredoski, Annie Moradian, Sonja Hess, Justin B. Kinney, and Rob Phillips. Systematic approach for dissecting the molecular mechanisms of transcriptional regulation in bacteria. *Proceedings of the National Academy of Sciences*, 115(21):E4796–E4805, May 2018. Publisher: National Academy of Sciences Section: PNAS Plus.

[54] Kaspar Valgepea, Kaarel Adamberg, Andrus Seiman, and Raivo Vilu. Escherichia coli achieves faster growth by increasing catalytic and translation rates of proteins. *Molecular BioSystems*, 9(9):2344–2358, July 2013. Publisher: The Royal Society of Chemistry.

[55] Alexander Schmidt, Karl Kochanowski, Silke Vedelaar, Erik Ahrné, Benjamin Volkmer, Luciano Callipo, Kèvin Knoops, Manuel Bauer, Ruedi Aebersold, and Matthias Heinemann. The quantitative and condition-dependent *Escherichia coli* proteome. *Nature Biotechnology*, 34(1):104–110, January 2016.

[56] Gene-Wei Li, David Burkhardt, Carol Gross, and Jonathan S. Weissman. Quantifying absolute protein synthesis rates reveals principles underlying allocation of cellular resources. *Cell*, 157(3):624–635, April 2014.

[57] Boumediene Soufi, Karsten Krug, Andreas Harst, and Boris Macek. Characterization of the *E. coli* proteome and its modifications during growth and ethanol stress. *Frontiers in Microbiology*, 6, February 2015. tex.ids: soufi2015a.

[58] Mehmet U. Caglar, John R. Houser, Craig S. Barnhart, Daniel R. Boutz, Sean M. Carroll, Aurko Dasgupta, Walter F. Lenoir, Bartram L. Smith, Viswanadham Sridhara, Dariya K. Sydykova, Drew Vander Wood, Christopher J. Marx, Edward M. Marcotte, Jeffrey E. Barrick, and Claus O. Wilke. The E. coli molecular phenotype under different growth conditions. *Scientific Reports*, 7(1):1–15, April 2017.

[59] Matteo Mori, Zhongge Zhang, Amir Banaei-Esfahani, Jean-Benoît Lalanne, Hiroyuki Okano, Ben C Collins, Alexander Schmidt, Olga T Schubert, Deok-Sun Lee, Gene-Wei Li, Ruedi Aebersold, Terence Hwa, and Christina Ludwig. From coarse to fine: the absolute *Escherichia coli* proteome under diverse growth conditions. *Molecular Systems Biology*, 17(5), May 2021.

[60] Mohan Babu, Cedoljub Bundalovic-Torma, Charles Calmettes, Sadhna Phanse, Qingzhou Zhang, Yue Jiang, Zoran Minic, Sunyoung Kim, Jitender Mehla, Alla Gagarinova, Irina Rodionova, Ashwani Kumar, Hongbo Guo, Olga Kagan, Oxana Pogoutse, Hiroyuki Aoki, Viktor Deineko, J. Harry Caufield, Erik Holtzapple, Zhongge Zhang, Ake Vastermark, Yogee Pandya, Christine Chieh-lin Lai, Majida El Bakkouri, Yogesh Hooda, Megha Shah, Dan Burnside, Mohsen Hooshyar, James Vlasblom, Sessandra V. Rajagopala, Ashkan Golshani, Stefan Wuchty, Jack F Greenblatt, Milton Saier, Peter Uetz, Trevor F Moraes, John Parkinson, and Andrew Emili. Global landscape of cell envelope protein complexes in Escherichia coli. *Nature Biotechnology*, 36(1):103–112, January 2018. Number: 1 Publisher: Nature Publishing Group.

[61] O Pierucci. Dimensions of Escherichia coli at various growth rates: model for envelope growth. *Journal of Bacteriology*, 135(2):559–574, August 1978. Publisher: American Society for Microbiology.

[62] A. Zaritsky and C. L. Woldringh. Chromosome replication rate and cell shape in *Escherichia coli*: lack of coupling. *Journal of Bacteriology*, 135(2):581–587, August 1978.

[63] F J Trueba and C L Woldringh. Changes in cell diameter during the division cycle of Escherichia coli. *Journal of Bacteriology*, 142(3):869–878, June 1980. Publisher: American Society for Microbiology.

[64] Arieh Zaritsky, Conrad L. Woldringh, Charles E. Helmstetter, and N. B. Grover. Dimensional rearrangement of Escherichia coli B/r cells during a nutritional shift-down. *Microbiology*, 139(11):2711–2714, 1993. Publisher: Microbiology Society,.

[65] N Grossman, E Z Ron, and C L Woldringh. Changes in cell dimensions during amino acid starvation of Escherichia coli. *Journal of Bacteriology*, 152(1):35–41, October 1982.

[66] H Bremer and Patrick P. Dennis. *Modulation of chemical composition and other parameters of the cell by growth rate. Neidhardt, et al. eds. Escherichia coli and Salmonella typhimurium: Cellular and Molecular Biology, 1st ed. chapter 96, Table 2 pp.1530-1*. Escherichia coli and Salmonella typhimurium: Cellular and Molecular Biology,. 1 edition, 1987.

[67] L. Arike, K. Valgepea, L. Peil, R. Nahku, K. Adamberg, and R. Vilu. Comparison and applications of label-free absolute proteome quantification methods on Escherichia coli. *Journal of Proteomics*, 75(17):5437–5448, September 2012.

[68] Abir T. Asmar, Josie L. Ferreira, Eli J. Cohen, Seung-Hyun Cho, Morgan Beeby, Kelly T. Hughes, and Jean-François Collet. Communication across the bacterial cell envelope depends on the size of the periplasm. *PLOS Biology*, 15(12):e2004303, December 2017. Publisher: Public Library of Science.

[69] Nathan M. Belliveau, Griffin Chure, Christina L. Hueschen, Hernan G. Garcia, Jane Kondev, Daniel S. Fisher, Julie A. Theriot, and Rob Phillips. Fundamental limits on the rate of bacterial growth and their influence on proteomic composition. *Cell Systems*, page S240547122100209X, July 2021.

[70] Ferhat Büke, Jacopo Grilli, Marco Cosentino Lagomarsino, Gregory Bokinsky, and Sander J. Tans. ppGpp is a bacterial cell size regulator. *Current Biology*, 32(4):870–877.e5, February 2022.

[71] Lisa U. Magnusson, Anne Farewell, and Thomas Nyström. ppGpp: a global regulator in Escherichia coli. *Trends in Microbiology*, 13(5):236–242, May 2005.

[72] Manlu Zhu, Yige Pan, and Xiongfeng Dai. (p)ppGpp: the magic governor of bacterial growth economy. *Current Genetics*, 65(5):1121–1125, October 2019.

[73] Katarzyna Potrykus and Michael Cashel. (p)ppGpp: Still Magical? *Annual Review of Microbiology*, 62(1):35–51, 2008. _eprint: https://doi.org/10.1146/annurev.micro.62.081307.162903.

[74] Beny Spira and Katia Ospino. Diversity in E. coli (p)ppGpp Levels and Its Consequences. *Frontiers in Microbiology*, 11, 2020.

[75] Kevin D. Young. The selective value of bacterial shape. *Microbiology and Molecular Biology Reviews*, 70(3):660–703, 2006.

[76] Nikola Ojkic, Diana Serbanescu, and Shiladitya Banerjee. Surface-to-volume scaling and aspect ratio preservation in rod-shaped bacteria. *eLife*, 8:e47033, aug 2019.

[77] T. E. Shehata and A. G. Marr. Effect of temperature on the size of Escherichia coli cells. *Journal of Bacteriology*, 124(2):857, November 1975. Publisher: American Society for Microbiology (ASM).

[78] Francis Mairet, Jean-Luc Gouzé, and Hidde de Jong. Optimal proteome allocation and the temperature dependence of microbial growth laws. *npj Systems Biology and Applications*, 7(1):1–11, March 2021. Number: 1 Publisher: Nature Publishing Group.

[79] Anne Farewell and Frederick C. Neidhardt. Effect of Temperature on In Vivo Protein Synthetic Capacity in *Escherichia coli*. *Journal of Bacteriology*, 180(17):4704–4710, September 1998.

[80] Benjamin D. Knapp and Kerwyn Casey Huang. The Effects of Temperature on Cellular Physiology. *Annual Review of Biophysics*, 51(1):499–526, May 2022.

[81] Abhishek Dey, Venkat Bokka, and Shaunak Sen. Dependence of bacterial growth rate on dynamic temperature changes. *IET Systems Biology*, 14(2):68–74, April 2020.

[82] Susana Matamouros, Thomas Gensch, Martin Cerff, Christian C. Sachs, Iman Abdollahzadeh, Johnny Hendriks, Lucas Horst, Niklas Tenhaef, Julia Tenhaef, Stephan Noack, Michaela Graf, Ralf Takors, Katharina Nöh, and Michael Bott. Growth-rate dependency of ribosome abundance and translation elongation rate in Corynebacterium glutamicum differs from that in Escherichia coli. *Nature Communications*, 14(1):5611, September 2023. Number: 1 Publisher: Nature Publishing Group.

[83] Johannes B. Müller, Philipp E. Geyer, Ana R. Colaço, Peter V. Treit, Maximilian T. Strauss, Mario Oroshi, Sophia Doll, Sebastian Virreira Winter, Jakob M. Bader, Niklas Köhler, Fabian Theis, Alberto Santos, and Matthias Mann. The proteome landscape of the kingdoms of life. *Nature*, 582(7813):592–596, June 2020. Number: 7813 Publisher: Nature Publishing Group.

[84] Sven van Teeffelen and Lars D. Renner. Recent advances in understanding how rod-like bacteria stably maintain their cell shapes. Technical Report 7:241, F1000Research, February 2018. Type: article.

[85] Ethan C. Garner. Toward a Mechanistic Understanding of Bacterial Rod Shape Formation and Regulation. *Annual Review of Cell and Developmental Biology*, 37(1):1–21, 2021. _eprint: https://doi.org/10.1146/annurev-cellbio-010521-010834.

[86] Patricia D.A. Rohs and Thomas G. Bernhardt. Growth and division of the peptidoglycan matrix. *Annual Review of Microbiology*, 75(1):315–336, 2021. PMID: 34351794.

[87] S. Anisah Alyahya, Roger Alexander, Teresa Costa, Adriano O. Henriques, Thierry Emonet, and Christine Jacobs-Wagner. Rodz, a component of the bacterial core morphogenic apparatus. *Proceedings of the National Academy of Sciences*, 106(4):1239–1244, 2009.

[88] Sven van Teeffelen, Siyuan Wang, Leon Furchtgott, Kerwyn Casey Huang, Ned S. Wingreen, Joshua W. Shaevitz, and Zemer Gitai. The bacterial actin mreb rotates, and rotation depends on cell-wall assembly. *Proceedings of the National Academy of Sciences*, 108(38):15822–15827, 2011.

[89] Cyrille Billaudeau, Arnaud Chastanet, Zhizhong Yao, Charlène Cornilleau, Nicolas Mirouze, Vincent Fromion, and Rut Carballido-López. Contrasting mechanisms of growth in two model rod-shaped bacteria. *Nature Communications*, 8(1):15370, Jun 2017.

[90] Nikolay Ouzounov, Jeffrey P. Nguyen, Benjamin P. Bratton, David Jacobowitz, Zemer Gitai, and Joshua W. Shaevitz. Mreb orientation correlates with cell diameter in escherichia coli. *Biophysical Journal*, 111(5):1035–1043, 2016.

[91] Alexandre Colavin, Handuo Shi, and Kerwyn Casey Huang. Rodz modulates geometric localization of the bacterial actin mreb to regulate cell shape. *Nature Communications*, 9(1):1280, Mar 2018.

[92] Randy M. Morgenstein, Benjamin P. Bratton, Jeffrey P. Nguyen, Nikolay Ouzounov, Joshua W. Shaevitz, and Zemer Gitai. RodZ links MreB to cell wall synthesis to mediate MreB rotation and robust morphogenesis. *Proceedings of the National Academy of Sciences*, 112(40):12510–12515, October 2015. Publisher: Proceedings of the National Academy of Sciences.

[93] Bob Carpenter, Andrew Gelman, Matthew D. Hoffman, Daniel Lee, Ben Goodrich, Michael Betancourt, Marcus Brubaker, Jiqiang Guo, Peter Li, and Allen Riddell. Stan: A probabilistic programming language. *Journal of Statistical Software*, 76(1):1–32, January 2017.

[94] Eric Soupene, Wally C. van Heeswijk, Jacqueline Plumbridge, Valley Stewart, Daniel Bertenthal, Haidy Lee, Gyaneshwar Prasad, Oleg Paliy, Parinya Charernnoppakul, and Sydney Kustu. Physiological studies of Escherichia coli strain MG1655: growth defects and apparent cross-regulation of gene expression. *Journal of Bacteriology*, 185(18):5611–5626, September 2003.

[95] D. Herbert, P.J. Phipps, and R.E. Strange. Chapter iii chemical analysis of microbial cells. volume 5 of *Methods in Microbiology*, pages 209–344. Academic Press, 1971.

[96] S. Benthin, J. Nielsen, and J. Villadsen. A simple and reliable method for the determination of cellular rna content. *Biotechnology Techniques*, 5(1):39–42, Jan 1991.

[97] Gilles Malherbe, David Paul Humphreys, and Emma Davé. A robust fractionation method for protein subcellular localization studies in *Escherichia coli*. *BioTechniques*, 66(4):171–178, April 2019.